Electronic Supporting Information

for

Nanoscale Rotational Dynamics of Four Independent Rotators Confined in Crowded Crystalline Layers

Antonio Rodríguez-Fortea,*[a] Enric Canadell,*[b] Pawel Wzietek,*[c] Cyprien Lemouchi,[d] Magali Allain,[e] Leokadiya Zorina,[e] and Patrick Batail*[d]

[a]*Departament de Química Física i Inorgànica, Universitat Rovira i Virgili, Marcel·li Domingo 1, 43007 Tarragona, Spain*
[b]*Institut de Ciència de Materials de Barcelona (ICMAB-CSIC), Campus de la UAB, 08193 Bellaterra, Spain*
[c]*Laboratoire de Physique des Solides, CNRS UMR 6502, Université de Paris-Sud, Orsay, France*
[d]*Laboratoire MOLTECH-Anjou, CNRS UMR 6200, Université d'Angers, 49045 Angers, France*
[e]*Institute of Solid State Physics, Russian Academy of Sciences, Chernogolovka MD, Russia*

email addresses of corresponding authors: antonio.rodriguezf@urv, canadell@icmab.es, pawel.wzietek@u-psud.fr and patrick.batail@univ-angers.fr

Experimental Section

Synthesis

The dissymmetric rod **1** was prepared as described previously.[1,2] Lithium hydroxide monohydrate (6 mg, 0.14 mmol) was added to a boiling methanol (5 mL) solution of **1** (50 mg, 0.14 mmol). Dimethylformamide (DMF, 15 mL) was added to the stirred solution. The clear solution was then cooled down to room temperature and stored in the dark for slow evaporation. After four days, colorless needles and plates were isolated after filtration and washed with cold DMF. Single-crystal X-ray diffraction was carried out on the plate-like crystals only on account of the poor diffracting properties of the needles.

Crystal structure

Crystal data at 120 K: $C_{102}H_{110}Li_4N_6O_{18}$, M = 1735.71 g mol^{-1}, triclinic, space group P-1, a = 11.098(2), b = 11.0981(9), c = 42.151(8) Å, α = 91.082(9), β = 97.390(10), γ = 115.846(8)°, V = 4617.1(13) Å^3, Z = 2, μ(MoKα) = 0.085 mm^{-1}, D_{calc} = 1.248 g/cm^3, 49460 reflections measured ($3.71 \leq 2\Theta \leq 50.18$), 14118 unique ($R_{int}$ = 0.0562, R_{sigma} = 0.0700) which were used in all calculations. The final R_1 was 0.0735 for 9216 reflections with $I > 2\sigma(I)$ and wR_2 was 0.2109 (all data). CCDC 1893363.

X-ray data were collected at 120 K using a Bruker Nonius KappaCCD diffractometer with monochromatized MoK_α-radiation (λ = 0.71073Å, graphite monochromator, combined φ/ω-scan). Empirical absorption correction was applied using the SADABS program.[3] The structure

was solved by a direct method followed by Fourier syntheses and refined by a full-matrix least-squares method in an anisotropic approximation for all non-hydrogen atoms using the SHELX-2016 programs.[4] Hydrogen atoms in water molecules were found from difference electron density maps and refined with restrained O-H and H-H distances and U_{iso}(H) fixed at 1.5U_{eq}(O). Other H-atoms were placed in idealized positions and refined in a riding model with U_{iso}(H) = 1.2U_{eq}(C). The crystal appeared to be a merohedral twin by a 180 º rotation about [1 1 0]. Twin fraction was refined to 0.126(1).

VT ^{1}H spin–lattice relaxation time (T_1)

Experiments were carried out as described previously[5,6] on a static crystalline powder at a ^{1}H Larmor frequencies of 55 MHz) and over a wide range of temperatures using a NMR spectrometer and probe built at Orsay. The probe is designed so as to reduce spurious proton signals. The polycrystalline sample was loaded into a small glass tube (typically 1.2 mm in diameter) upon which the NMR coil was wound. ^{1}H signals were recorded using the FID following a $\pi/2$ pulse (typically 0.8-1.5 μs) and spin-lattice relaxation was measured using the standard saturation recovery sequence. For each T_1 measurement we recorded signals for 20 values of the relaxation delay between the saturating comb and the measuring pulse.

Details of the fitting procedure

It is of interest to note that BCO units and methyl groups of the DMF molecules being chemically different moving parts, obviously with different structures, their relaxations are different and cannot be scaled one versus the other.

As shown in Figure 5, one single line is drawn over the T_1^{-1} data points; this fit contains two contributions (see Table S1 which summarizes the fit coefficients for Me and BCO) implemented as follows:

The two methyl peaks (those at low temperature, see Figure 5) were fitted using equation 9 in Allen and Clough paper.[18] Note that both peaks could be fitted using a single normalization constant which strongly supports the assignment of these peaks to the methyl groups.

Table S1. Parameters used in the fit (solid line in Figure 5) of the ^{1}H spin-lattice relaxation time, T_1^{-1} to the Kubo-Tomita expression. The first two parameters E_a and τ_0 are related to BCO rotators. Other parameters provided by equation (9) in Allen and Clough[18] describe the classical and quantum dynamics of a methyl group in the solid state.

E_a	3000 K	6.0 kcal mol^{-1}
τ_0	1.6 x 10^{-13} s	
E_c	1000 K	2.0 kcal mol^{-1}
τ_c	4.6 x 10^{-13} s	
E_t	460 K	0.9 kcal mol^{-1}
τ_t	6.9 x 10^{-13} s	
J	9.6 MHz	
C	3.11 10^8	

Then, for the high T part, the overall amplitude (that is the constant C in the Kubo-Tomita formula) was not fitted. Instead, the normalization was calculated using the following scaling procedure:

From Kubo-Tomita (equations 1 and 2 in the main text) it is seen that for a given C value the amplitude of the $1/T_1$ peak, noted hereafter $[1/T_1]$max, is inversely proportional to the Larmor frequency ω_n. Therefore, the quantity $[1/T_1]\text{max}/\omega_n$ will be proportional to the ratio of the number of moving protons (Figure S1c) contributing to the peak over the total number of protons yielding a proportionality constant that does not depend on the material studied providing the rotor is the same chemical unit and the spin temperature well defined. This property enables one to calculate the normalization constant using experimental data obtained for a different BCO system.

To demonstrate this procedure, here is how it works on two different BCO systems published recently, namely **2**[7] and **3**[5]:

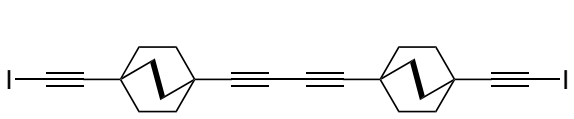

2

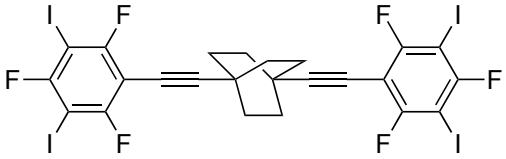

3

For **2** (ref 7), $[1/T_1]$max amounts to 16.3 s^{-1} at 62 MHz for 24 moving BCO protons and 8 static protons. For **3** (ref 5), a material with no static protons, $[1/T_1]$max amounts to 24 s^{-1} at 55MHz. Therefore the expected $[1/T_1]$max for **2**, scaled from the data of system **3**, will be 24 s^{-1} x 24/(24+8) x 55/62 = 16 s^{-1} which matches closely the measured value 16 s^{-1}. This is seen as compelling evidence that this procedure is reliable.

The same procedure is now used to scale our data (compound **1**) versus **3**. The expected $[1/T_1]$max = 24 s^{-1} x 48/(48+62) x 55/57 = 10.1 s^{-1}. Therefore the Kubo-Tomita contribution to the global fit was normalized so that $[1/T_1]$max = 10.1 s^{-1}.

We conclude that the fact that the normalization constant was independently determined makes for a reliable determination of the rotational barrier E_a. We estimate its uncertainty to be within 0.3 kcal mol^{-1} .

Computational Details

Partial optimizations. Calculations were performed as described previously[5,6,7,8] using the hybrid M06-2X functional[9] and the 6-31G(d,p) basis set[10] as implemented in the Gaussian09 package.[11]

Car-Parrinello molecular dynamics. All the simulations were carried out using the CPMD code.[12,13] The simulations for the small rotors layer (Figure 4a) were performed in a monoclinic box with vectors a = (11.098 Å, 0.000 Å, 0.000 Å), b = (-4.838 Å, 9.988 Å, 0.000 Å) and c = (-2.711 Å, -1.755 Å, 20.827 Å). The core electrons were described by Troullier-Martins norm-

conserving pseudopotentials.[14] The electronic potential was calculated by means of the PBE density functional[15] using a plane waves basis set with a cut-off of 40 Ry. The time step was set to 0.120 fs and the fictitious electron mass to 600 au. The system was first equilibrated at 300 K using the Nosé-Hoover chain thermostat.[16,17] A production run of 300 ps at 300 K was done. We have activated such small rotors model system performing a first metadynamics run in which we have considered a single collective variable, one H-C-C-C dihedral angle (see Figure 4a). The mass and the coupling constant of the collective variable (CV) were M = 10 a.u. and k = 0.5 a.u. The height of the hills was W = 0.031 kcal mol^{-1}, their perpendicular width $\Delta s^{\perp}$ = 0.05 rad and the deposition rate Δt = 0.012 ps. The total simulation time was t_{total} = 51 ps. A second metadynamics run considering two dihedral angles for two different rotors (the two nearest rotors in the unit cell) as collective variables was also done for the small model. The masses and coupling constants for the two CVs were $M_1 = M_2$ = 10 a.u. and $k_1 = k_2$ = 0.5 a.u. The height of the hills was W = 0.063 kcal mol^{-1}, their perpendicular width $\Delta s^{\perp}$ = 0.05 rad and the deposition rate Δt = 0.012 ps. The total simulation time was t_{total} = 840 ps.

Finally, we have performed an analogous study with a more realistic system in which the terminal groups of the rotor are kept. In fact, the benzoate and the pyridine of each rotor are modeled each by a benzene ring (large rotors model, see Figure S4). Simulations were performed in a monoclinic box with vectors *a* = (11.098 Å, 0.000 Å, 0.000 Å), *b* = (-4.838 Å, 9.988 Å, 0.000 Å) and c = (-4.066 Å, -2.633 Å, 31.240 Å). The time step was set now to 0.144 fs. A metadynamics run considering two dihedral angles for two different large rotors (the two nearest rotors in the unit cell) as collective variables was done for this large model. The masses and coupling constants for the two CVs were $M_1 = M_2$ = 10 a.u. and $k_1 = k_2$ = 0.5 a.u. The height of the hills was W = 0.314 kcal mol^{-1}, their perpendicular width $\Delta s^{\perp}$ = 0.05 rad and the deposition rate Δt = 0.0144 ps. The total simulation time was t_{total} = 360 ps.

Figure S1. a) Representative element symbols complementing Figure 1b. The two DMF molecules are located near the Li^+ tetrahedra, far enough from the BCO rotators that they should not significantly affect their dynamics (shorter C–H•••H–C distances: 2.66 Å and 2.67 Å); b) Coordinative structure around the lithium cation; c) Chemical structure and inventory of the static and moving Hs.

Figure S2. Colorless plate-like crystal used for X-ray data collection.

Figure S3. Position of an arbitrary C atom of each of the rotors along the long metadynamics trajectory of the unit cell with four small rotors (Figure 6a). The blue and red positions correspond to the activated rotations (small rotors A and B) whereas the black and green positions to the non-activated ones (small rotors C and D).

Figure S4. Unit cell with four large rotors used in the Car-Parrinello MD simulations.

Figure S5. (a) Position of an arbitrary C atom of each of the rotors along the whole trajectory of the unit cell with four large rotors (Figure 6b). The blue and red positions correspond to the activated rotations (large rotors A and B), whereas the black and green positions to the non-

activated ones (large rotors C and D). (b) Scheme representing two neighbor rotors with their two sets of positions, 1 and 2, separated by a rotation of 60 degrees.

Figure S6. Enlarged view of two portions of the long metadynamics trajectory for the set of four small rotors (Figure 6a). Some of the different types of rotations have been highlighted.

Figure S7. Enlarged views of two portions of the metadynamics trajectory with large rotors in Figure 6b. Some of the different types of rotations have been highlighted. See the movie (large_model_longMD_335_340ps.mp4) corresponding to part (a).

Table S1. Parameters used in the fit (solid line in Figure 6) of the ^{1}H spin-lattice relaxation time, T_1^{-1} to the Kubo-Tomita expression. E_a and τ_0 are related to BCO rotators. Other parameters provided by equation (9) in Allen and Clough[a] describe the classical and quantum dynamics of a methyl group in the solid state.

Two movies:

"small_model_shortMD_39_47ps.mp4" (movie 1) and
"large_model_longMD_335_340ps.mp4" (movie 2) associated with Figures 4 and S7, respectively.

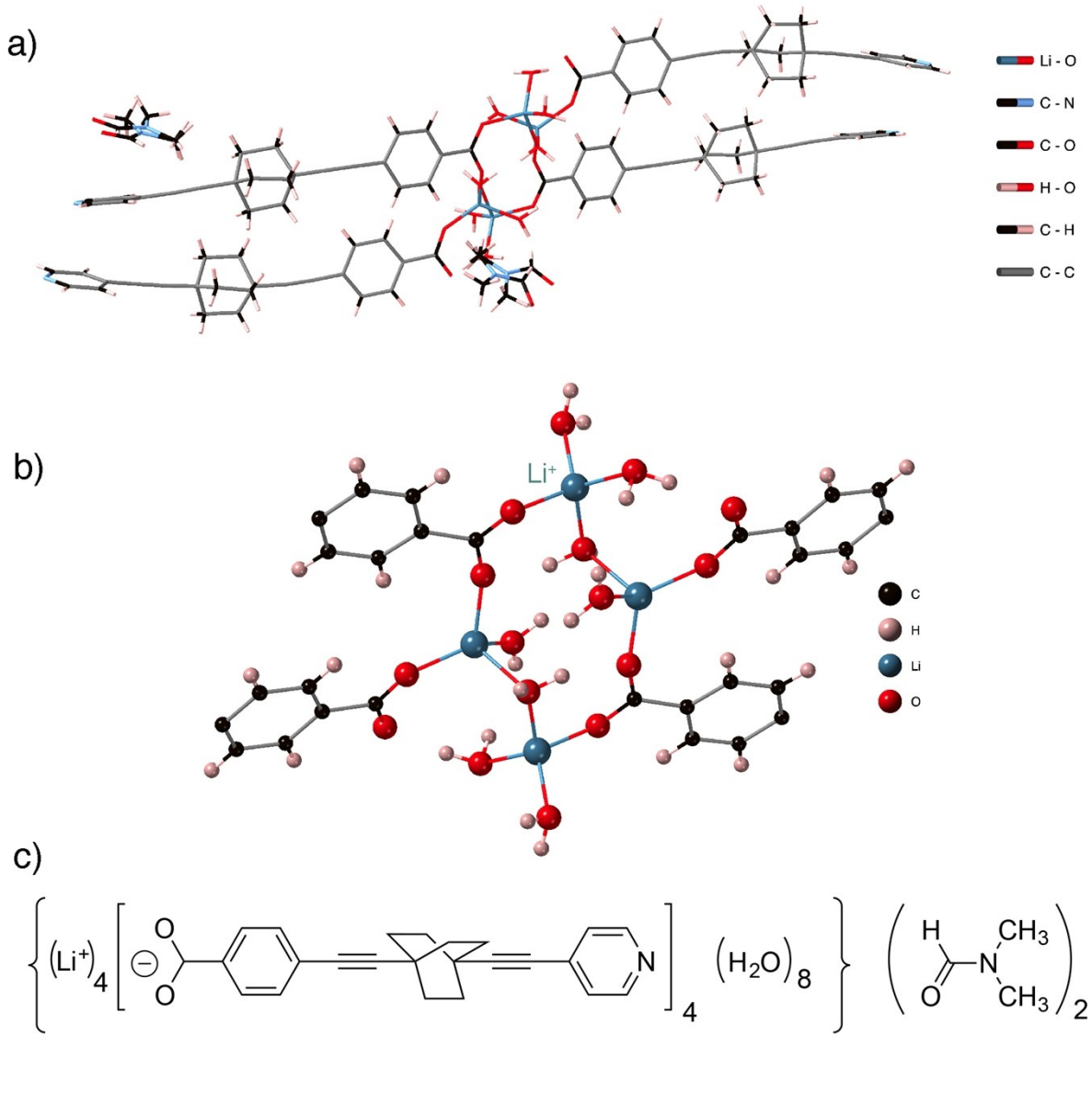

Figure S1. a) Representative element symbols complementing Figure 1b. The two DMF molecules are located near the Li^+ tetrahedra, far enough from the BCO rotators that they should not significantly affect their dynamics (shorter C–H•••H–C distances: 2.66 Å and 2.67 Å); b) Coordinative structure around the lithium cation; c) Chemical structure and inventory of the static and moving Hs.

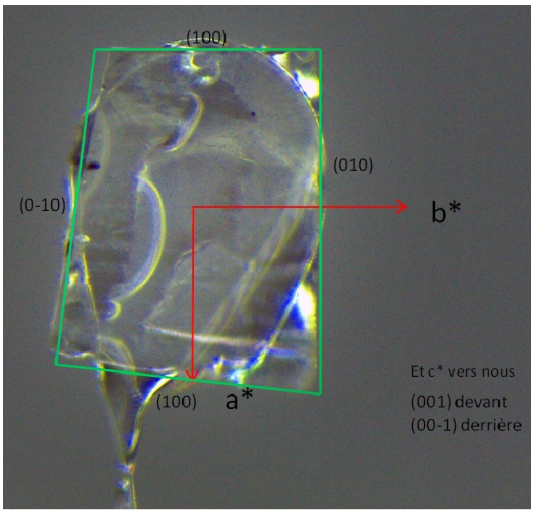

Figure S2. Colorless plate-like crystal used for X-ray data collection.

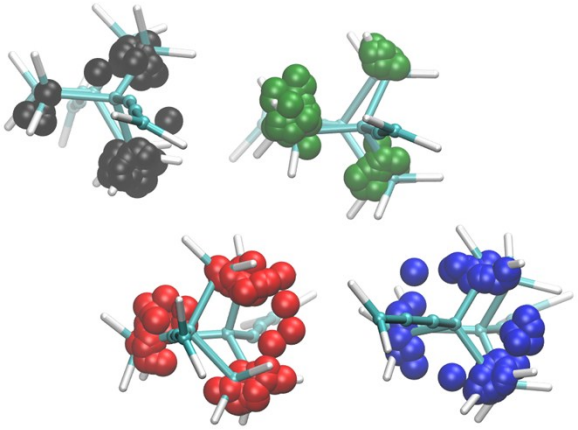

Figure S3. Position of an arbitrary C atom of each of the rotors along the long metadynamics trajectory of the unit cell with four small rotors (Figure 6a). The blue and red positions correspond to the activated rotations (small rotors A and B) whereas the black and green positions to the non-activated ones (small rotors C and D).

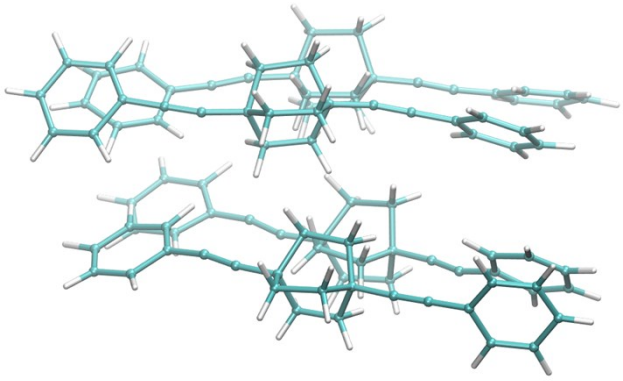

Figure S4. Unit cell with four large rotors used in the Car-Parrinello MD simulations.

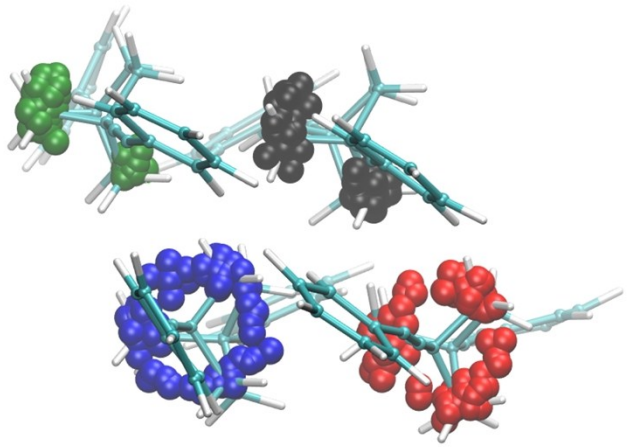

(a)

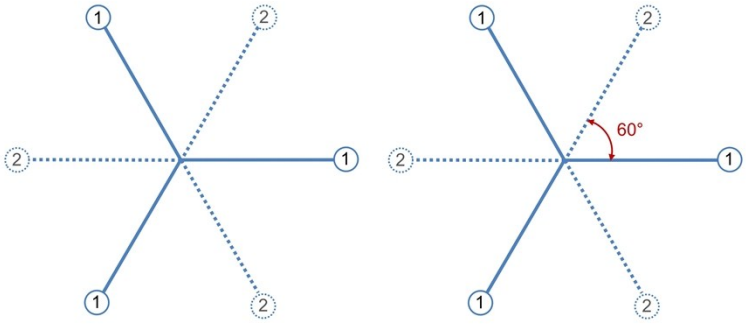

(b)

Figure S5. (a) Position of an arbitrary C atom of each of the rotors along the whole trajectory of the unit cell with four large rotors (Figure 6b). The blue and red positions correspond to the activated rotations (large rotors A and B), whereas the black and green positions to the non-activated ones (large rotors C and D). (b) Scheme representing two neighbor rotors with their two sets of positions, 1 and 2, separated by a rotation of 60 degrees.

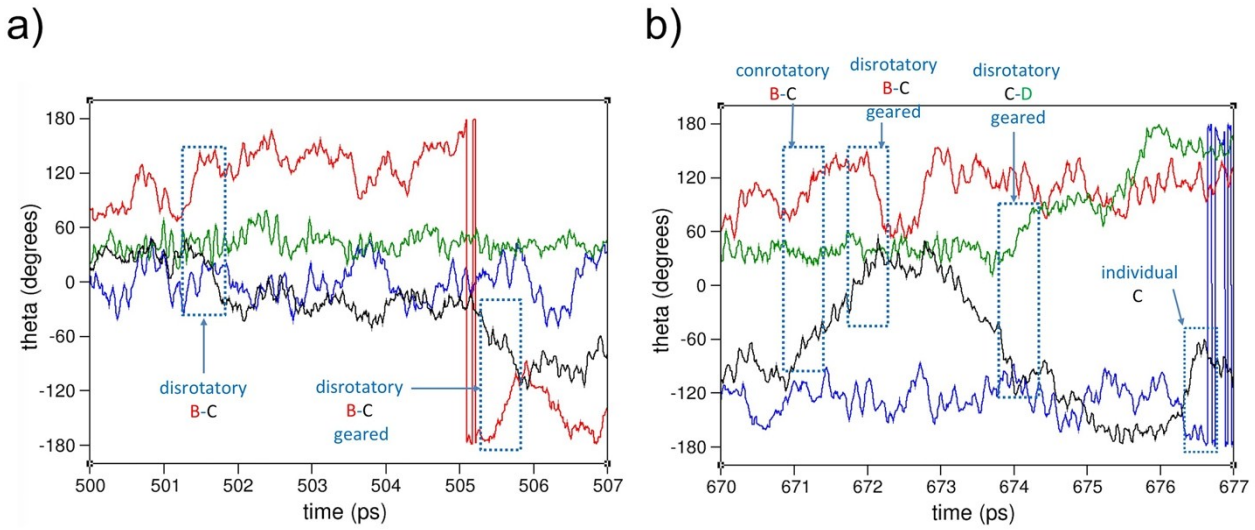

Figure S6. Enlarged view of two portions of the long metadynamics trajectory for the set of four small rotors (Figure 6a). Some of the different types of rotations have been highlighted. Rotors A and B are activated and rotors C and D are not activated.

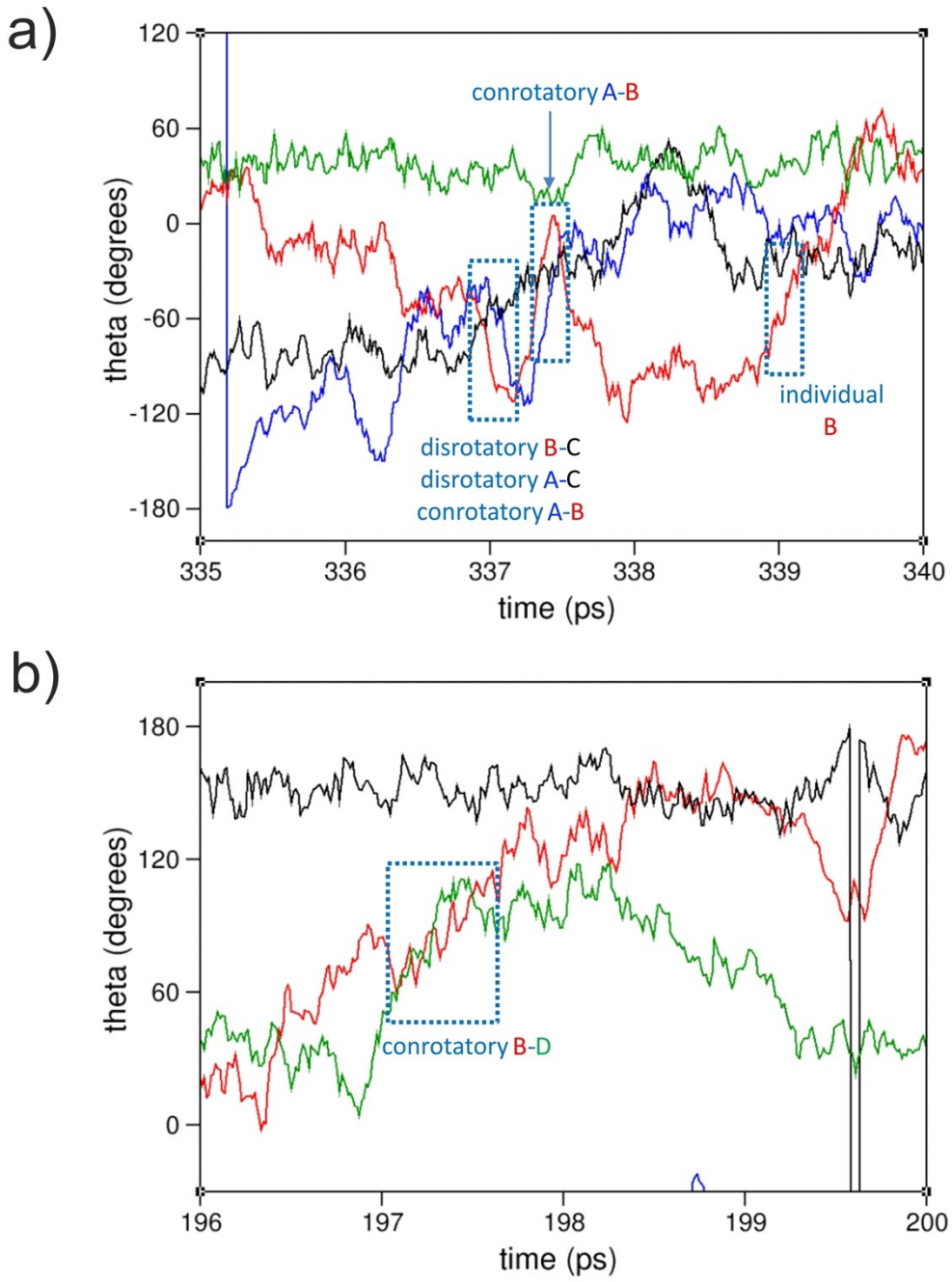

Figure S7. Enlarged view of two portions of the metadynamics trajectory with large rotors in Figure 6b. Some of the different types of rotations have been highlighted. Rotors A and B are activated and rotors C and D are not activated. See the movie (large_model_longMD_335_340ps.mp4) corresponding to part (a) in the Supplementary Information.

References

1 C. Lemouchi, P. Batail, *Beilstein J. Org. Chem.* 2015, **11**, 1881-1885.

2 G. M. Locke, S. S. R. Bernhard, M. O. Senge, *Chem. Eur. J.* 2019, **25**, 4590-4647.

3 SADABS, version 2008/1, Bruker (2008), Bruker AXS Inc., Madison, Wisconsin, USA.

4 G. M. Sheldrick, *Acta Cryst.* 2008, **A64**, 112-122.

5 C. Lemouchi, H. M. Yamamoto, R. Kato, R.; S. Simonov, S.; L. Zorina, L.; A. Rodríguez-Fortea, A.; E. Canadell, E.; P. Wzietek, K. Iliopoulos, D. Gindre, M. Chrysos, P. Batail, *Cryst. Growth Des.* 2014, **14**, 3375-3383.

6 C. Lemouchi, C. Mézière, L. Zorina, S. Simonov, A. Rodríguez-Fortea, E. Canadell, P. Wzietek, P. Auban-Senzier, C. Pasquier, T. Giamarchi, M. A. Garcia-Garibay, P. Batail, P., *J. Am. Chem. Soc.* 2012, **134**, 7880-7891.

7 C. Lemouchi, I. Iliopoulos, L. Zorina, S. Simonov, P. Wzietek, P.; T. Cauchy, A. Rodríguez-Fortea, E. Canadell, J. Kaleta, J. Michl, D. Gindre, M. Chrysos, P. Batail, P., *J. Am. Chem. Soc.* 2013, **135**, 9366-9376.

8 G. Bastien, C. Lemouchi, M. Allain, P. Wzietek, A. Rodríguez-Fortea, E. Canadell, K. Iliopoulos, D. Gindre, M. Chrysos, P. Batail, *CrystEngComm* 2014, **16**, 1241-1244.

9 Y. Zhao, D. G. Truhlar, *Theor. Chemica Acta.* 2008, **120**, 215-241.

10 P. C. Hariharan, J. A. Pople, *Theor. Chimica Acta*, 1973, **28**, 213-222.

11 Gaussian 09, Revision B1, M. J. Frisch, G. W. Trucks, H. B. Schlegel, G. E. Scuseria, M. A. Robb, J. R. Cheeseman, G. Scalmani, V. Barone, B. Mennucci, G. A. Petersson, H. Nakatsuji, M. Caricato, X. Li, H. P. Hratchian, A. F. Izmaylov, J. Bloino, G. Zheng, J. L. Sonnenberg, M. Hada, M. Ehara, K. Toyota, R. Fukuda, J. Hasegawa, M. Ishida, T. Nakajima, Y. Honda, O. Kitao, H. Nakai, T. Vreven, J. A. Montgomery Jr.; J. E. Peralta, F. Ogliaro, M. Bearpark, J. J. Heyd, E. Brothers, K. N. Kudin, V. N. Staroverov, R. Kobayashi, J. Normand, K. Raghavachari, A. Rendell, J. C. Burant, S. S. Iyengar, J. Tomasi, M. Cossi, N. Rega, J. M. Millam, M. Klene, J. E. Knox, J. B. Cross, V. Bakken, C. Adamo, J. Jaramillo, R. Gomperts, R. E. Stratmann, O. Yazyev, A. J. Austin, R. Cammi, C. Pomelli, J. W. Ochterski, R. L. Martin, K. Morokuma, V. G. Zakrzewski, G. A. Voth, P. Salvador, J. J. Dannenberg, S. Dapprich, A. D. Daniels, Ö. Farkas, J. B. Foresman, J. V. Ortiz, J. Cioslowski, D. J. Fox, Gaussian, Inc., Wallingford CT, 2009.

12 R. Car, M. Parrinello, *Phys. Rev. Lett.* 1985, **55**, 2471-2474.

13 CPMD v3.15; Copyright MPI für Festkörperforschung: Stuttgart, Germany, 1997-2001, Copyright IBM Corp. 1990-2011.

14 N. Troullier, J. L. Martins, *Phys. Rev. B* 1991, **43**, 1993.

15 J. P. Perdew, K. Burke, M. Ernzerhof, *Phys. Rev. Lett.* 1997, **78**, 1396.

16 S. Nosé, *J. Chem. Phys.* 1984, **81**, 511.

17 W. G. Hoover, *Phys. Rev. A* 1985, **31**, 1695.

18 P. S. Allen, S. Clough, *Phys. Rev. Lett*. 1969, **22**, 1351-1353.